J Infrared Milli Terahz Waves (2012) 33:797–815
DOI 10.1007/s10762-012-9913-y

Terahertz Properties of Graphene

Callum J. Docherty · Michael B. Johnston

Received: 24 January 2012 / Accepted: 24 May 2012 /
Published online: 9 June 2012

Abstract Graphene has proved itself as being unique in terms of fundamental physics, and of particular importance for post–silicon electronics. Research into graphene has divided into two branches, one probing the remarkable electronic and optical properties of graphene, and the other pursuing technologically viable forms of the material. Terahertz time domain spectroscopy (THz TDS) is a powerful tool for both, able to characterise the free carrier response of graphene and probe the inter and intraband response of excited carriers with sub-ps time resolution. We review THz TDS and related THz measurements of graphene.

Keywords Graphene · Terahertz time domain spectroscopy · Graphite · Conductivity

1 Introduction

Graphene, a flat monolayer of carbon atoms forming a two-dimensional (2D) honeycomb structure, has been named 'the simplest complex material' [1]. It exhibits mobilities in excess of any observed in conventional bulk semiconductors [2], and allows the observation of relativistic quantum mechanics on a condensed matter scale [3], but can be produced using Scotch tape [4]. The first isolation of a monolayer of graphene in 2004 by the now Nobel prize winning Geim and Novoselov transformed the material from a theoretical model, deemed by Landau and Peierls to be unstable at all finite temperatures

C. J. Docherty · M. B. Johnston (✉)
Department of Physics, Clarendon Laboratory, University of Oxford,
Parks Road, Oxford, OX1 3PU, UK
e-mail: M.Johnston@physics.ox.ac.uk

[5], into a practical reality [4]. Since then graphene has been touted for use as future field effect transistors [6], the replacement for indium tin oxide (ITO) in touch screens [7], electrodes in solar cells [8], and even as anti-bacterial paper [9].

The unique properties of graphene fuel the great enthusiasm for the material. Graphene has shown ballistic transport at room temperature [2] with massless Dirac fermions as the carriers [3], an anomalous quantum Hall effect [10], Klein tunnelling [11], and immense tensile strength [12], to name but a few. However, the electronic properties of graphene, particularly the dynamics of hot carriers, must be understood before graphene can be utilised fully for optoelectronic devices [13].

Terahertz Time Domain Spectroscopy (THz TDS) is a method well placed for such studies [14]. This all–optical technique can probe the intrinsic carrier dynamics in the time domain, undisturbed by the influence of contacts that would otherwise have to be attached [15]. Coupled with a higher energy excitation pulse, ultrafast carrier relaxation can be observed with sub–ps time resolution.

Here we review previous results of THz TDS and related spectroscopies on graphene. This review is organised as follows: Section 2 describes the various forms of graphene that have been studied; Section 3 reviews work on the equilibrium dynamics of graphene; Section 4 describes investigations of photoexcited carrier dynamics by optical pump–optical probe spectroscopy, optical pump–THz probe spectroscopy, and theoretical work.

2 Production of graphene

Graphene is not a uniform term. Each of the various methods of producing graphene yields a product that is distinct, with a drop in mobility being particularly noticeable in the more up–scalable techniques. Thus when comparing spectroscopic investigations, the type of graphene, and its likely form and quality, must be considered. Furthermore, many of the production methods are still in their infancy, with great improvements in quality and domain size of product in recent years. Therefore, two studies on nominally similar graphene could be investigating very different materials.

In the decades preceding the first isolation of graphene, several attempts were made to produce a single layer of graphite, already predicted to have special properties [16]. As far back as 1960, Fernandez-Moran had mechanically exfoliated ~ 15 layers of graphene in a search for electron microscopy support membranes [17]. Iijima used adhesive tape to cleave graphite crystals for the same purpose, foreshadowing Geim and Novoselov's successful method, but then used ethylene dichloride to separate the flakes and leave them in suspension [18]. Other researchers attempted the reduction of oxidized graphite [19], with little success. Later attempts included the use of an AFM cantilever to peel off a single layer, again without success [20].

In the context of these complicated attempts to isolate a monolayer of graphene, the simplicity of Geim and Novoselov's Scotch tape method of producing mechanically exfoliated graphene stands out [4]. Their success in 2004 fuelled both the experimental exploration of graphene, and renewed interest in previously unsuccessful production methods. Epitaxial growth of graphene rapidly followed, and since then the reduction of graphene oxide, liquid-phase exfoliation and chemical vapour deposition have shown promise as large-scale means of producing graphene for technological exploitation.

2.1 Mechanical exfoliation

Geim and Novoselov's method utilised common adhesive tape to apply the weak force (300 $nN/\mu m^2$ [21]) required to overcome the inter-layer Van der Waals interaction in graphite [4]. The resulting pieces of graphite and graphene were transferred to a silicon dioxide substrate, where contrast between the substrate and graphene allows the observation of a monolayer. In this way, pristine mono- and few-layer graphene was isolated, and used to investigate graphene's electronic properties.

Presently mechanical exfoliation yields the best quality graphene, with extremely high mobilities [22]. However, its production is time consuming, and not viable on a large scale. In order to utilise graphene's electronic properties in low cost applications, focus has shifted from mechanical exfoliation to chemical methods of production, despite the resulting loss of quality of graphene.

2.2 Epitaxial growth

An early contender to mechanical exfoliation, epitaxial growth of graphene involves the thermal treatment of silicon carbide SiC (0001), resulting in the sublimation of the Si atoms, and a reorganisation and graphitisation of the carbon-enriched surface to form layers of graphene [23]. The observation of graphene's properties on these samples, notably the anomalous quantum Hall effect, led to the initial belief that monolayers of graphene were formed on the SiC surface [24]. However, Raman and STM studies have since shown that this is not the case, and in fact 10-20 layers are produced [25]. This should prohibit the observation of graphene like properties, as graphitic AB stacking breaks the equivalence of the two atoms in the graphene lattice. Fortunately, rotational stacking faults develop during the growth process, which electronically decouple the layers from one another, and so gives the effect, and electronic properties of, a monolayer.

Originally, epitaxial graphene was grown at 1300°C under vacuum [24]. Graphene prepared in such a way, however, had very limited lateral extension of graphene crystallites, adversely affecting the electronic capabilities of the material. This issue was resolved by the graphitisation of Si-terminated SiC (0001) in a 900 mbar argon atmosphere [26]. At the higher temperature required for Si to sublime under this condition (1500°C as opposed to 1150°C in vacuo), surface diffusion is enhanced such that the surface reorganisation

occurs before the graphene is formed. Thus much larger domains of graphene form, with a resulting increase of mobility to 2000 cm^2/Vs at 27 K. The improvement of domain size using this method can be seen in Fig. 1a and b. Whilst this mobility seems modest in comparison to mechanically exfoliated graphene, where mobility can exceed 200,000 cm^2/Vs [27], it is sufficient to make epitaxially grown graphene useful for field-effect devices, and the nature of the graphene on an insulating SiC substrate allows easy integration into electronic devices. However, there are many defects, non-uniformities and high intrinsic doping in the graphene, limiting the performance of any devices using this production route. Additionally, the system is only quasi-2D, the layers are not entirely decoupled, and cannot be transferred to a different substrate. Thus, other production methods are needed.

2.3 Chemical vapour deposition (CVD)

One of the most promising production methods for large-scale technological application of graphene is chemical vapour deposition. It had long been

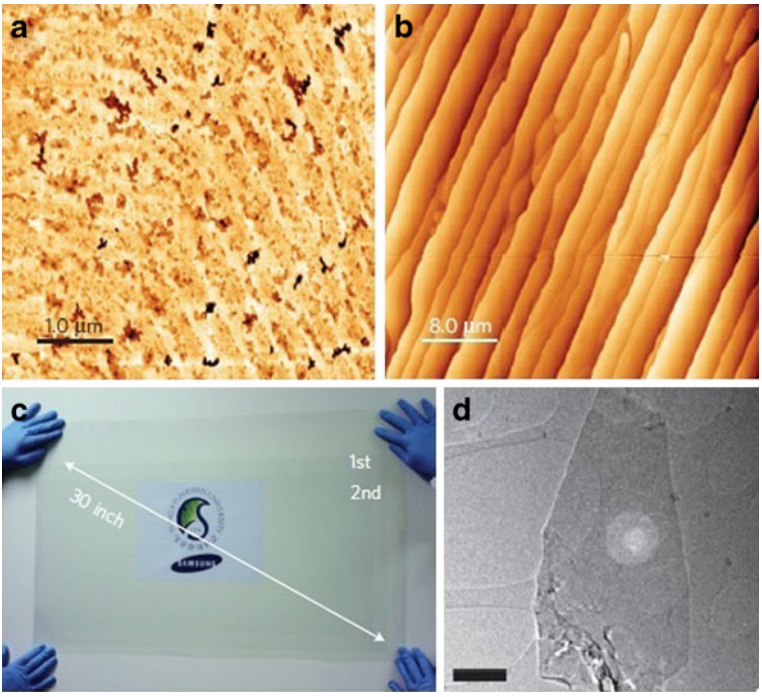

Fig. 1 **a**, **b** AFM images of epitaxial graphene grown (**a**) in vacuo and (**b**) in an argon atmosphere. The increased lateral size is clear in (**b**). Reprinted by permission from Macmillan Publishers Ltd: Nat. Mat. [26]. ©(2009). **c** 30 inch CVD graphene sheet. Reprinted by permission from Macmillan Publishers Ltd: Nat. Nanotechnol. [28] © (2010). **d** TEM image of liquid–phase exfoliated monolayer (scale bar 500 nm). Reprinted by permission from Macmillan Publishers Ltd: Nat. Nanotechnol. [29]. ©(2008).

known that CVD of hydrocarbons on transition metal surfaces could produce thin graphitic layers [30]. Inspired by this, graphene growth using CVD was attempted, using ethylene as the carbon source, and ruthenium as the substrate [31]. Domains of graphene exceeding 100 μm were formed in this way, but the strong metal–graphene interaction limited both further lateral extension, and carrier transport.

More recently, Bae *et al.* [28], managed to grow 30-inch sheets of predominantly monolayer graphene on flexible copper substrates (Fig. 1c), yielding $\sim 125\,\Omega$ per square sheet resistance, and 97.4% transparency. HNO_3 was used to hole dope the sheets even further than the usual p doping found in CVD graphene, lowering the sheet resistance of four stacked graphene layers to $\sim 30\,\Omega$ per square, three times less than indium tin oxide (ITO), the material currently used in touch screens. It is thus highly likely that this method will be used to replace ITO electrodes, particularly in view of the limited world supply of indium. Indeed, the same group, working in collaberation with Samsung, have produced an example touch screen device utilising graphene.

Despite these promising results, CVD fabrication remains linked to expensive templates, which are only relevant for high performance applications, such as the devices requiring touch screens [19]. For lower cost, lower performance applications, wet chemical approaches offer an alternative route.

2.4 Wet chemical routes

Whereas mechanical exfoliation utilises tape to overcome the Van der Waals interaction between graphene layers in high quality graphite crystals, wet chemicals can weaken these interlayer forces by inserting reactants into the interlayer space, and so drive exfoliation [32]. As these methods are carried out in suspension, they can be easily applied to large-scale manufacture. A number of wet chemical processes have so far been shown to yield graphene, including reduction of graphene oxide [32–35], and liquid-phase exfoliation [29, 36, 37].

Wet chemical approaches yield graphene with mobilities at least two orders of magnitude smaller than mechanically exfoliated graphene, more impurities, and smaller domain sizes (Fig. 1d) [36, 38]. However, they are methods in their infancy, and improved results can be anticipated for the future.

3 Terahertz transmission and equilibrium conductivity of graphene

It is well known that at visible wavelengths, the absorbance of a graphene monolayer is $\pi\alpha$, where α is the fine structure constant, independent of wavelength, due to a constant optical conductivity of $\pi e^2/2h$ [39]. In the THz regime, however, a Drude absorption peak is expected due to free carriers [40]. This prediction has been tested on both CVD and epitaxially grown graphene, using both THz TDS and far-IR Fourier transform interferometer (far-IR FTIR) spectroscopy [40–43].

Dawlaty *et al.* with epitaxial graphene [41], and Lee *et al.* [40] and Horng *et al.* [42] with CVD grown graphene utilised FTIR to investigate transmission and hence conductivity in the THz–Far-IR range. These investigations all found the conductivity of graphene to be Drude-like in the THz regime, indicating the dominance of intraband conductivity over interband at low frequencies. A typical result can be seen in Fig. 2.

Horng *et al.* in particular tested the validity of the predicted Drude behaviour. According to a Drude model, the conductivity should have the form $\sigma = [iD/\pi(\omega + i\Gamma)]$, where ω is the frequency, Γ the scattering rate, and D the Drude weight. For the Dirac fermions in graphene, this has a value $D = (v_F e^2/\hbar)\sqrt{\pi|n|}$, with $v_F = 1.1 \times 10^6\,\mathrm{ms}^{-1}$ the Fermi velocity and $|n|$ the carrier density. This is in contrast to the usual Drude weight in classical materials of $D = \pi n e^2/m^*$.

In order to test this prediction, a gate voltage was applied to the sample to linearly alter the carrier density from the intrinsic hole doping of CVD grown graphene [4]. It was found that at all carrier densities, the measured D was lower than predicted. This difference could be explained by electron-electron interactions, ignored in the Boltzmann transport theory derivation of D. However, one theoretical study investigating this correction predicted a much larger reduction of the Drude weight than observed by Horng *et al.* Alternatively, defect induced electron or hole localisation could lower the effective free carrier concentration, accounting for the reduced Drude weight. Further investigation is needed to determine the cause of the discrepancy.

In addition to these FTIR measurements, Tomaino *et al.* utilised THz time domain spectroscopy to map the carrier dynamics of a large area CVD sample on a silicon substrate with > 90% monolayer coverage [43]. THz transmission through the sheet as a function of position was measured, and used to deduce the local sheet conductivity, σ_s. They measured an inhomogeneity in σ_s of between 1.7×10^{-3} and 2.4×10^{-3} S, which they ascribed to variations in

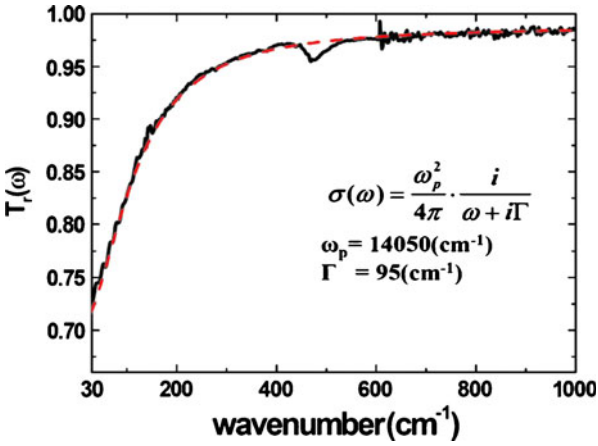

Fig. 2 Typical transmission spectrum of graphene. The increased absorption at THz wavelengths indicates a Drude type conductivity. At higher wavelengths, the absorption approaches the constant $\pi\alpha$. Reproduced with permission from [40]. ©American Institute of Physics 2011.

doping level. These conductivity values are 30 times greater than the constant conductivity at optical wavelengths, suggesting intraband transitions dominate the conductivity, in agreement with FTIR studies. This hypothesis was confirmed by an agreement between the THz conductivity and dc conductivity measured using a four probe technique. This work highlighted the benefits of using THz spectroscopy as a contactless probe of conductivity.

A Fourier transform of these THz TDS results yielded the frequency dependent transmission through the sample. Tomaino *et al.* found a flat, featureless response up to the the experimental bandwidth of 2 THz, suggesting the probe frequencies were well below the Drude roll-off frequency, in contrast to the FTIR measurements described above.

In a further THz TDS study on CVD-grown graphene, Maeng *et al.* [44] utilised a gate voltage to modulate the carrier density, similarly to Horng *et al.* [42]. The optical conductivity was again found to be spectrally flat, with the magnitude of conductivity related to the carrier density. When the Fermi level was tuned to be close to the Dirac point, so that carrier density was minimal, the conductivity was observed to be independent of n at room temperature. Away from the Dirac point, however, the optical conductivity varied as $\sqrt{n}$. Both of these observations can be explained within a Drude framework, in the two separate regimes of low and high carrier density. Additionally, chemical doping using viologen [45] was used to reduce the p-type doping of the CVD-grown graphene, and shown to have an identical effect to modulation of the carrier density by applying a gate voltage.

There has been little investigation of the discrepancy between these spectrally flat THz TDS results and the FTIR measurements. A further FTIR study by Choi *et al.* on both mono and multilayer epitaxially grown graphene samples indicated that the Drude roll-off frequency for monolayer samples was higher, and the conductivity drop much smaller than for the multilayer sample [46]. Thus the quality of the sample potentially effects the observed conductivity form.

4 Pump-probe spectroscopy

An alternative form of spectroscopy, pump-probe spectroscopy, allows the time domain investigation of excited carrier dynamics. An understanding of the ultrafast relaxation dynamics of carriers in graphene is essential for designing new graphene-based optoelectronic devices [47]. An optical pump pulse (usually $\lambda \sim 800$nm) is used to photoexcite the sample, and a weaker probe pulse is subsequently used to map the cooling of these hot carriers with sub-ps resolution by comparing the transmission of the probe beam with and without the excitation pulse. By using a THz probe, the ultrafast relaxation dynamics of low energy carriers near the Dirac point can be studied. However, most work so far has used higher energy IR probes, and so we briefly review these studies here.

4.1 Optical pump–optical probe

The first studies of graphene using this method utilised the then new epitaxial growth method for producing samples. Dawlaty *et al.* investigated samples with between 6 and 37 layers of epitaxial graphene, using a 780 nm pump and probe beam [48]. They found that upon excitation, probe transmission increased rapidly (photo-induced bleaching) due to state blocking, followed by a relaxation on two distinct exponential time scales, as seen in the bottom section of Fig. 3. A first, fast relaxation time of 70–120 fs was followed by a slower time of 0.4–1.7 ps. The first time scale was attributed to the equilibration of the photoexcited carrier populations by carrier-carrier intraband scattering. A subsequent thermalisation by carrier-phonon scattering was attributed to the longer time constant. A schematic of this relaxation can be seen in top section of Fig. 3.

Later works utilised a longer wavelength probe, but found broadly similar results to Dawlaty *et al.* [48], differing only in the interpretation of the cooling mechanisms. Newson *et al.* studied mechanically exfoliated graphene of varying layer number [49]. A similar two time constant decay was found, with the longer time scale attributed to a mixture of carrier-phonon and carrier-carrier scattering. Additionally, it was found that the results were similar for 1–3 layers of graphene. For more the 3 layers, however, the second time constant was found to lengthen, highlighting the importance of inter-layer interactions. Hale *et al.* [50] and Wang *et al.* [47] observed the familiar two time constant decay on exfoliated and CVD grown graphene respectively, but interpreted the longer decay as a bottleneck in cooling due to anharmonic decay of hot optical phonons. Ruzicka *et al.* demonstrated that the diffusion

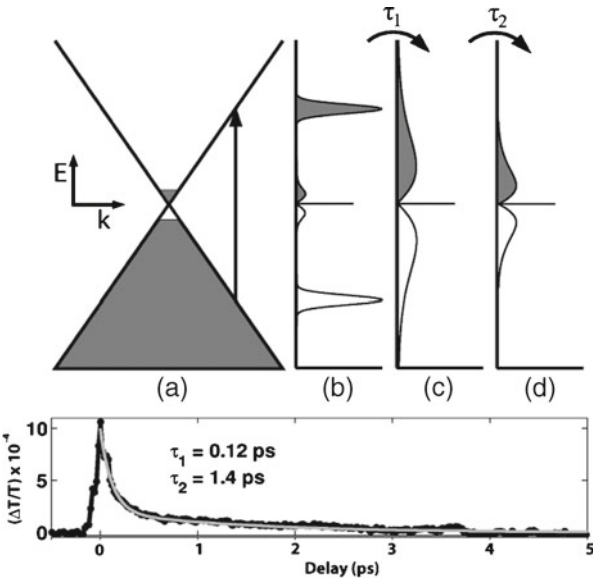

Fig. 3 *Top* **a** Band structure of graphene showing effect of optical pump. **b** Distribution of carriers immediately after pump. **c** Equilibration of carriers by carrier-carrier scattering. **d** Subsequent cooling of hot carrier distribution by carrier-phonon scattering or recombination. *Bottom* Typical transmittivity transient seen in optical pump-probe experiments. Decay is characterised by two time constants, τ_1 and τ_2. Reproduced with permission from [48]. ©American Institute of Physics 2008.

coefficients in epitaxially grown graphene and reduced graphene oxide (RGO) differed by only a factor of two ($1.1 \times 10^4\,\mathrm{cm^2 s^{-1}}$ and $5.5 \times 10^3\,\mathrm{cm^2 s^{-1}}$ respectively) [51]. This is an encouraging result, considering the low cost of RGO fabrication. Other than this result, however, there have been few direct comparisons between different types of graphene.

Optical pump–probe spectroscopy can yield important information about carrier dynamics. However, the high energy optical probe primarily examines interband transitions in graphene. To investigate the intraband response, terahertz (THz) length radiation is preferable [13].

4.2 Optical–pump terahertz–probe spectroscopy

Due most likely to the relative novelty of THz techniques [52], even fewer investigations have utilsed a THz rather than optical or IR probe beam, and of these epitaxially grown graphene has been tended to be used. As a result of this preference, results have mainly been performed on a number of graphene layers, rather than a monolayer.

Kampfrath *et al.* studied a sample consisting of enough layers of graphene to be considered graphite [53]. The 17 nm thick graphite had the same linear dispersion relation around the Dirac point as graphene, and so the optical pump provided the same excitation as was shown in Fig. 3. A 780 nm femtosecond Ti:sapphire laser oscillator was used both to excite the sample, and to generate THz pulses from frequency mixing in a GaSe crystal, yielding a spectral range of 8 to 30 THz.

In the experiment, the THz signal through the graphite film was sampled as a function of pump-probe delay time, τ, and the associated change in complex dielectric function, $\Delta\varepsilon_\tau$ determined. As a function of time, the THz signal decayed in a similar manner to the optical probe experiments discussed previously. In the frequency domain, it was found (Fig. 4), that the imaginary part of ε_τ, and hence the transmittivity, increased below 15 THz (photo-induced bleaching), but decreased above that (photo-induced absorption). It was concluded that this effect can be explained by the interplay between direct optical transitions (DOTs) and indirect optical transitions involving a change in carrier momentum (IOTs). Specifically, exciting the sample with the pump pulse transfers electrons to the conduction band. After 0.5 ps, the hot electrons thermalise, and can be described by a Fermi-Dirac distribution with electronic temperature T_e. The newly created electron-hole pairs block some DOTs, limiting the absorption of photons of energy $\sim k_\mathrm{B} T_e$. Simultaneously, however, the hot distribution enables additional IOTs, hence increasing the absorption in the THz range.

For further analysis, the IOT change in dielectric function was modelled using Drude formalism: $\varepsilon^{\mathrm{IOT}} = -\omega_{\mathrm{pl}}^2/(\omega^2 + i\gamma\omega)$, where γ is the Drude relaxation rate. By comparing the electronic temperature T_e to the equivalent temperature of the pump photons (1200 K), it was observed that within the pump-probe delay time of 500 fs, the electron distribution cools rapidly, losing more than 90% of its initial energy. This was considered to be in part due

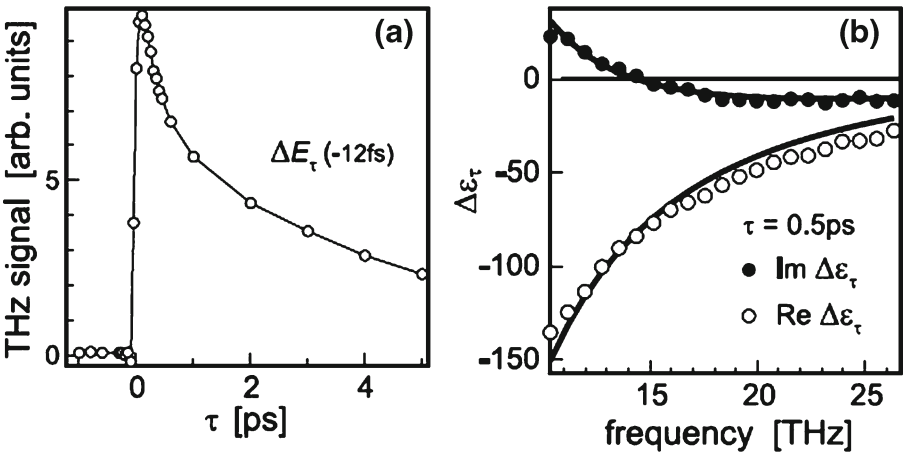

Fig. 4 **a** Change in THz electric field as a function of pump probe delay, τ. **b** Pump induced changes in complex dielectric function at $\tau = 0.5$ps after photoexcitation. Reproduced with permission from [53]. ©American Physical Society 2005.

to strong coupling of the electrons to hot phonons, though such strongly coupled optical phonons (SCOPs) could not account entirely for the cooling (see Fig. 5). This conclusion mirrors the hot phonon bottleneck explanation of Hale *et al.* and Wang *et al.* discussed previously [47, 50]. The remaining cooling could have been due to carrier-carrier scattering, as was proposed for the rapid cooling observed previously by Dawlaty *et al.* [48]. Kampfrath concluded that the increased relaxation rate from the SCOPs may limit the performace of graphene in electric circuits.

The first time resolved THz study on true graphene was performed by George *et al.* [13]. Two epitaxially grown graphene samples were investigated: sample B consisting of ∼12 carbon atom layers, and sample C of ∼20 layers [13]. Raman spectroscopy, an important tool in the analysis of the quality of graphene [54], showed that sample C contained significantly more disorder

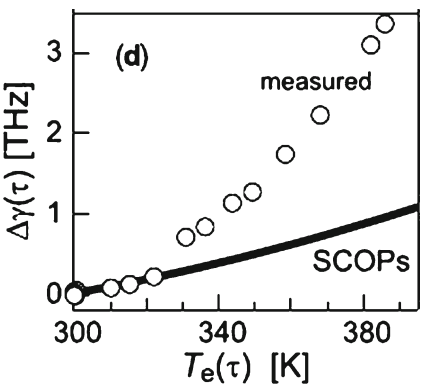

Fig. 5 Pump induced changes in scattering rate $\Delta\gamma(\tau)$ against electronic temperature T_e. The *black line* is the theoretical result for purely SCOP scattering. That this is much lower than the measured result shows SCOPs cannot be solely responsible for the rapid cooling of photoexcited electrons. Reproduced with permission from [53]. ©American Physical Society 2005.

than sample B. The layers adjacent to the SiC substrate had a much larger carrier density than the further out, intrinsic layers. It was found that the intrinsic layers dominated the change in terahertz intraband conductivity, so that the adjacent layers could be safely ignored in the analysis.

George *et al.* utilised a photo-conductive switch [55], and electro-optic sampling [56], to produce and detect pulses with bandwidth 0.3–3 THz. The graphene was excited by 90 fs pulses from a 780 nm Ti:sapphire laser, delivering 1–16 nJ of energy to a 350 μm spot size. It was found that the photoexcitation of graphene increased the absorption of the THz field, but did not cause a time delay in the transmission of the pulse. In frequency space, this corresponds to a flat, dispersionless real photo-induced conductivity with a negligible imaginary part. This is a result of the ultrafast momentum relaxation time in graphene, and is common to all the THz-TDS studies working in this low frequency range. Therefore, all such works have tracked only the peak of the THz pulse as a function of pump-probe delay time, rather than investigating the full photo-induced conductivity spectrum.

George *et al.* found that transmittivity through the graphene as a function of probe delay showed an initial rapid decrease, caused by an increase in conductivity due to the cooling of the thermalised carrier distribution, followed by a slower, few picosecond, non-exponential increase resulting from first intraband phonon scattering, then electron-hole recombination (Fig. 6). Thus the optically pumped electrons are once again behaving as in the schematic in Fig. 3.

Possible recombination mechanisms could include a combination of plasmon emission, phonon emission and Auger scattering. The recombination processes were modelled using simple coupled rate equations, expressing the recombination rate as a quadratic function of electron density n, $R(n) = B(n^2 - n_{\mathrm{eq}}^2)$, where n_{eq} is the carrier density at thermal equilibrium, and B is a fitting function. For sample B, a constant value of $1.8\,\mathrm{cm^2 s^{-1}}$ for B was found to provide a good theoretical model for the observed reflectivity (see black line in Fig. 6). Thus recombination rates depend on carrier density. For sample C, the value was 3.1. The recombination rate for sample C was twice that of sample B, showing that increased disorder increases recombination rates. The calculated recombination rates were ~ 2 times higher than that predicted for Auger scattering alone [57], suggesting multiple recombination mechanisms are involved. The model was also well able to take into account the increased initial transmission drop when higher pump pulses were used to excite the samples.

In a similar work, Choi *et al.* used THz TDS to investigate fewer layers of epitaxial graphene than George *et al.*, comparing nominally monolayer graphene and multilayer (~ 5 layers) [46]. Low-energy electron microscopy (LEEM), angle-resolved photoemission spectroscopy (ARPES), and scanning tunnelling microscopy (STM) [58, 59] showed the monolayer sample to consist of single-crystalline nanoribbon-like terraces of monolayer graphene, with widths from 60 to 250 nm. These comparatively small widths are characteristic of early epitaxially grown graphenes (see Section 2.2).

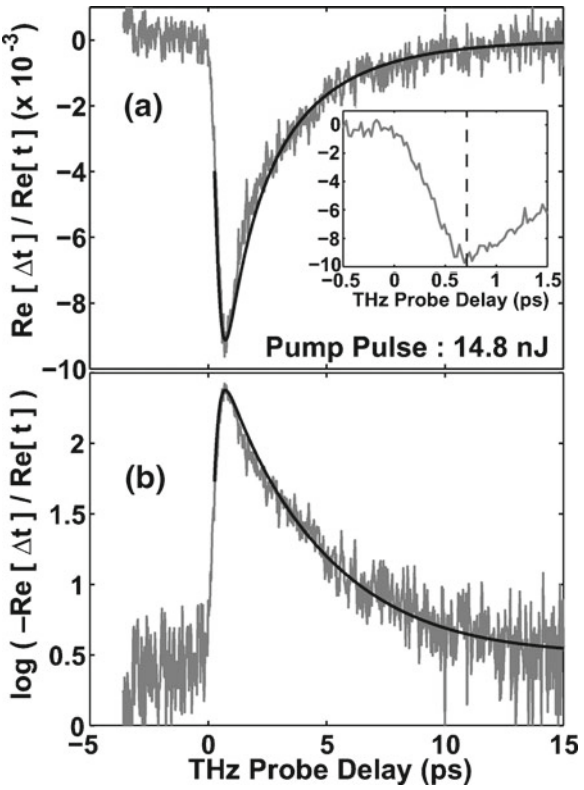

Fig. 6 **a** The measured change in the real part of the complex amplitude transmission (*grey*), and theoretical model (*black*). Inset: Closer view of inital rapid fall. **b** The same data on a logarithmic scale, showing that the slow decay is not exponential. Reproduced with permission from [13]. ©American Chemical Society 2008.

Choi *et al.* employed 500 μm thick ZnTe crystals for both optical rectification [60] and electro-optic sampling to produce and detect THz pulses with bandwidth 0.5–3 THz [61]. An 800 nm Ti:sapphire regenerative amplifier was used to pump both the THz generation and the graphene samples, resulting in a maximum incident fluence of 0.9 μJ/cm^2 on the samples. Once again, only the transmission of the peak of the THz pulse through the graphene was tracked, due to the dispersionless nature of the material.

In contrast to George *et al.*, a monoexponential decay of the photo-induced absorption was observed for both mono and multilayer samples (Fig. 7). In such few layer epitaxial samples, the graphene is highly n-doped by the substrate, unlike thicker samples where the THz response is dominated by the undoped layers away from the substrate. Thus the THz response can reflect changes in minority and majority carriers.

To model their monoexponential absorption decay, Choi *et al.* assumed a monoexponential decay of photoexcited carrier density $n = p = p_0 \exp(-t/\tau_R)$ where $p_0 = n_0 = 4.6 \times 10^{10}\,\mathrm{cm}^{-2}$ is the initial photoexcited carrier density corresponding to a pump fluence of 0.9 μJ/cm^2, and τ_R =1.3 ps and 1.2 ps for mono and multilayer graphene respectively. For a given carrier temperature,

this allowed the photo-induced conductivity for electrons and holes to be calculated.

By comparison of the observed data to this model, it was found that the hole contribution to this conductivity far outweighed the electronic contribution. Furthermore, allowing for cooling of the carrier temperature had little effect on the calculated conductivity. Thus the THz response is dominated by the recombination of the minority hole carriers, with a largely fluence independent recombination time $\tau_R \simeq 1.2$ ps. This time is consistent with that predicted for Auger and phonon-mediated recombination by some theoretical works [57].

More recent theoretical work on carrier recombination has suggested characteristic time scales shorter than one picosecond could be observed, particularly plasmon scattering [62–64]. To investigate the inconsistency of experimental results with theoretical behaviour, Strait *et al.* performed THz TDS on 14-layer epitaxially grown graphene at different substrate temperatures [65]. Terahertz pulses were produced and detected using photoconductive antennas, and the sample excited by 780 nm, 11.4 nJ pump pulses with spot size 1 mm^2.

Upon excitation of the sample with the pump beam, the THz transmission fell sharply, similarly to previous investigations, with a system resolution lim-

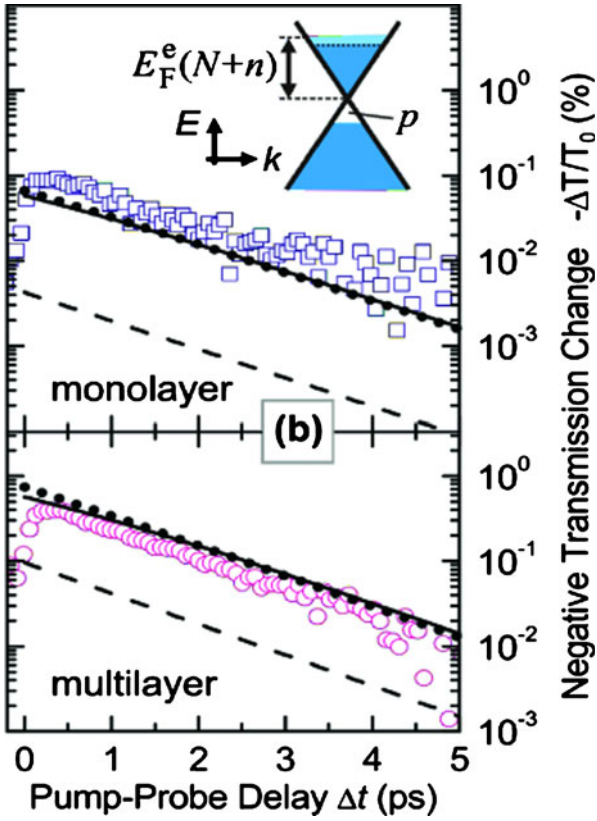

Fig. 7 Monoexponential decay of photo-induced absorption in mono- and multilayer graphene observed by Choi *et al.* The *dashed (dotted) lines* represents the electron (hole) contribution from their conductivity model, showing the dominance of the hole response. Reproduced with permission from [46]. ©American Institute of Physics 2009.

ited time scale of ~ 1 ps (Fig. 8). The transmission then recovered over a period of tens of picoseconds at room temperature, but hundreds of picoseconds at low substrate temperatures. At these low temperatures, two distinct time scales are clear, a first, 'fast' recovery lasting around 50 ps, then a much longer recovery lasting hundreds of picoseconds. Additionally, the magnitude of the peak pump induced transmission change ($|\Delta T|$) is of greater magnitude at lower substrate temperatures.

These observations were modelled using rate equations. Immediately after photoexcitation, the hot carriers were assumed to thermalise by carrier-carrier scattering (as in Fig. 3), leaving the carriers in Fermi-Dirac distributions with well defined Fermi Levels, E_{fe} and E_{fh} for electrons and holes respectively. The subsequent evolution of electron, hole and phonon distributions was then modelled, incorporating previously published models for optical phonon scattering [47, 63], Auger scattering [57], acoustic phonon scattering [66] and plasmon decay [62]. This model accounted well for the observed data, and suggested the following mechanism for carrier cooling:

Immediately after thermalisation, optical phonon generation rapidly cools the initially large carrier temperature. For times < 1 ps, E_{fh} is greater than E_{fe}, and so the carrier generation rate exceeds the carrier recombination rate, increasing the electron and hole densities. This generation also assists in carrier cooling. This accounts for the increase of photo-induced absorption (and hence also photo-induced conductivity) up to 1 ps. After 1 ps, the situation is reversed, $E_{\mathrm{fe}} > E_{\mathrm{fh}}$, and so carrier population decreases and optical phonon scattering reduces the photo-induced absorption.

The generation of optical phonons in this initial period gradually raises the temperature of the phonon distribution, until the rising optical phonon temperatures and the falling carrier temperatures match. As the carrier distributions cool further, inter- and intraband scattering by optical phonons becomes inefficient. As scattering by acoustic phonons is also inefficient in graphene [67, 68], this causes a bottleneck in the cooling, and accounts for the slowing of the recovery of the THz transmission, an explanation similar to that of the more recent optical pump–optical probe measurements [47, 50].

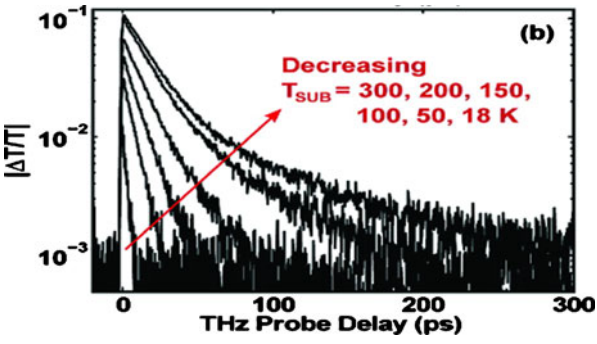

Fig. 8 The differential THz probe transmission measured by Strait *et al.* as a function of pump probe delay time and substrate temperature, shown on logarithmic scale. Two time constants can clearly be seen at lower substrate temperatures. Reproduced with permission from [65]. ©American Chemical Society 2011.

The experiment was re-run on a graphene sample consisting of 30 layers, yielding almost identical results, despite more than doubling the thickness of the sample. These results show the importance of optical phonons in graphene-based optical and electronic devices, with the relatively high energy of optical phonons in graphene (0.196 and 0.162 eV [54]) standing out in comparison to other semiconductors.

Terahertz spectroscopy has thus been put to good use investigating the cooling of photoexcited carriers in graphite and epitaxial graphene. The four papers discussed here have shown broadly similar results: photo-induced absorption of low photon energy probes (as opposed to the photo-induced bleaching observed in optical pump-optical probe experiments), a rapid change upon photoexcitation, and a room temperature relaxation over a few picoseconds. However there are still some differences in the interpretation of cooling mechanisms, perhaps related to the different samples investigated, which range from nanoribbon-like monolayers to many layered graphite.

4.3 Theoretical results and THz lasing

In addition to the experimental results described above, some authors have published theoretical works on the terahertz conductivity of graphene. In particular, Ryzhii *et al.* used a model incorporating both the inter- and intra-band conductivities to calculate the frequency response of optically excited graphene [69]. Treating the photoexcited carriers as quickly thermalising to a Fermi distribution, as observed in the previous sections, and using a Drude mechanism, they calculated the real part of the conductivity, which is proportional to the absorption coefficient of the graphene. Their results are shown for weak pumping in Fig. 9, for various values of optical pump intensity, at a temperature of 77 K. This is therefore the form of conductivity that a THz TDS investigation of graphene could expect to see. They further showed that under strong pumping, population inversion can be achieved, resulting in a negative net conductivity in the THz range, and hence negative absorption coefficient. Experimental observations of this behaviour have recently been reported [70]. Thus it may be possible to use graphene as a coherent source of THz radiation utilising stimulated photon emission - it could be possible to use graphene as a THz laser.

Following this work, Rana has shown the potential application of graphene for plasmon amplification [71]. Plasmons, charge density waves, have been shown to be in the THz range in graphene [72]. Utilising the population inversion of Ryzhii *et al.*, Rana has provided a model for potential plasmon oscillation. A step towards the realisation of this model was accomplished by the recent frequency tuning of plasmons in graphene micro-ribbons by Ju *et al.* [73].

Other theoretical works have highlighted the potential influence of intense THz radiation on the electrical properties of graphene. Wright *et al.* demonstrated the strong nonlinearity of single layers of intrinsic graphene [74]. When subjected to a sufficiently strong, but experimentally achievable,

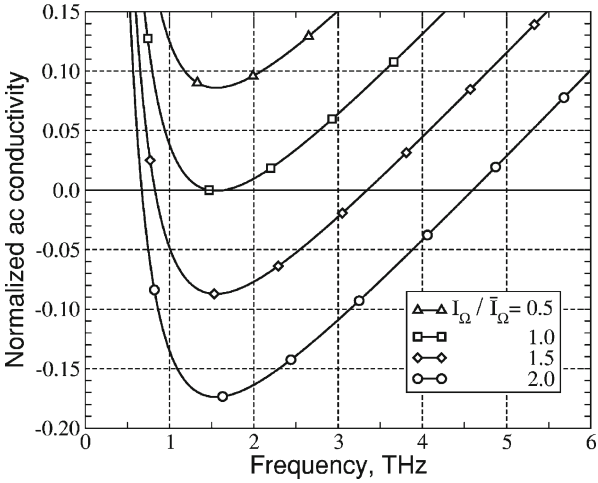

Fig. 9 Frequency dependence of normalised real part of the ac conductivity of graphene as a function of frequency, for different intensities of optical pump radiation. Reproduced with permission from [69]. ©American Institute of Physics 2007.

terahertz electic field, third order terms in the induced photocurrent become significant. In particular, their model suggests that a THz frequency tripling term is important at room temperature. Such behaviour would enable THz frequency upcoversion device applications.

A similar conclusion was drawn by Bao *et al.* [75]. Using a model considering impurity, acoustic phonon and optical phonon scattering in graphene driven by intense terahertz radiation, these authors also highlighted the effect of the THz field on the linear conductivity of the graphene. They noted that the dc mobility of the graphene always decreases under THz irradiation, with the decrease greater for strong THz fields and lower frequencies. This effect may be important for future THz devices, and could even be used as a method of frequency sensitive detection of THz radiation. Other works have also suggested this potential application for graphene. Liu *et al.* predicted a distinctive frequency dependent variation in conductivity due to the incident THz radiation [76], whilst Jiang *et al.* found large, frequency dependent peaks in the THz conductivity of a graphene sheet tuned by a periodic gate voltage [77].

Many of these theoretical predictions have yet to be tested experimentally, but this is to be expected from a material such as graphene, which is still in its infancy. More work is required to unite experiment and theory, to understand the properties of graphene and move towards real world applications.

5 Concluding remarks

Since its discovery, graphene has been extensively studied for potential wide ranging use in the future. Through dc conductivity measurements, graphene has proved to be a unique material, displaying near ballistic transport, a half-integer quantum Hall effect, and opening a new frontier in ‘relativistic’ condensed matter physics. A variety of optical methods have been refined to

characterise graphene sheets, with optical microscopy in particular standing ready to control large scale production.

Having shown its intrinsic remarkable properties with mechanically exfoliated graphene, research into cheaper and more technologically applicable production methods has surged. Epitaxial growth, CVD and wet chemical routes all show promise for some applications, but fail for others. Promisingly, these methods show no signs of reaching their fundamental capabilities, and further advances can be anticipated, particularly with wet chemicals.

THz time domain spectroscopy, in combination with other ultrafast spectroscopies, has expanded our understanding of carrier dynamics in graphene. Work so far has shed light on the inherent ac conductivity of graphene, without a need for contacts, and the interplay between various possible cooling methods of excited carriers. The strengths that can make graphene useful in a wide range of future applications are highlighted by such works, as are the limitations of graphene that must be understood before graphene devices can be successfully implemented. There is still much work to be done. Firstly, the assumption that graphene is always a perfect two–dimensional crystal in isolation from its environment is, in most cases, not valid. There are significant challenges faced by materials scientists to improve graphene growth techniques. Furthermore, in order to understand experimental observations, theoretical models need to consider the messy interactions between graphene and its environment. Secondly ultrafast charge carrier dynamics in graphene are yet to be fully understood and exploited. This challenge will need to be overcome to realise terahertz frequency devices based on graphene. Indeed most device applications of graphene remain suggestions rather than demonstrated capabilities. However, these are still the early days of graphene research. In the coming years, THz spectroscopic methods will play a key role in the development of graphene–based materials and devices. In particular these techniques can probe the high–frequency response of graphene, provide feedback on production methods and test the operation of new devices.

Acknowledgement The authors would like to thank the EPSRC for financial support.

References

1. A. Bostwick, J. McChesney, T. Ohta, E. Rotenberg, T. Seyller, K. Horn, Prog. Surf. Sci. **84**, 380 (2009)
2. X. Du, I. Skachko, A. Barker, E.Y. Andrei, Nat. Nanotechnol. **3**, 491 (2008)
3. K.S. Novoselov, A.K. Geim, S.V. Morozov, D. Jiang, M.I. Katsnelson, I.V. Grigorieva, S.V. Dubonos, A.A. Firsov, Nature **438**, 197 (2005)
4. K.S. Novoselov, A.K. Geim, S.V. Morozov, D. Jiang, Y. Zhang, S.V. Dubonos, I.V. Grigorieva, A.A. Firsov, Science **306**, 666 (2004)
5. A.K. Geim, K.S. Novoselov, Nat. Mater. **6**, 183 (2007)
6. Y.M. Lin, C. Dimitrakopoulos, K.A. Jenkins, D.B. Farmer, H.Y. Chiu, A. Grill, P. Avouris, Science **327**, 662 (2010)
7. S. De, J.N. Coleman, ACS Nano **4**, 2713 (2010)
8. M.H. Liang, B. Luo, L.J. Zhi, Int. J. Energy Res. **33**, 1161 (2009)

9. W.B. Hu, C. Peng, W.J. Luo, M. Lv, X.M. Li, D. Li, Q. Huang, C.H. Fan, ACS Nano **4**, 4317 (2010)
10. Y.B. Zhang, Y.W. Tan, H.L. Stormer, P. Kim, Nature **438**, 201 (2005)
11. N.M.R. Peres, J. Phys.-Condes. Matter **21**, 323201 (2009)
12. C. Lee, X.D. Wei, J.W. Kysar, J. Hone, Science **321**, 385 (2008)
13. P.A. George, J. Strait, J. Dawlaty, S. Shivaraman, M. Chandrashekhar, F. Rana, M.G. Spencer, Nano Lett. **8**, 4248 (2008)
14. R. Ulbricht, E. Hendry, J. Shan, T.F. Heinz, M. Bonn, Rev. Mod. Phys. **83**, 543 (2011)
15. R. Golizadeh-Mojarad, S. Datta, Phys. Rev. B **79**, 085410 (2009)
16. A.H.C. Neto, F. Guinea, N.M.R. Peres, K.S. Novoselov, A.K. Geim, Rev. Mod. Phys. **81**, 109 (2009)
17. H. Fernandez-Moran, J Appl Phys **31**, 1844 (1960)
18. S. Iijima, Micron **8**, 41 (1977)
19. C. Soldano, A. Mahmood, E. Dujardin, Carbon **48**, 2127 (2010)
20. T.W. Ebbesen, H. Hiura, Adv. Mater. **7**, 582 (1995)
21. Y.B. Zhang, J.P. Small, W.V. Pontius, P. Kim, Appl. Phys. Lett. **86**, 073104 (2005)
22. K.I. Bolotin, K.J. Sikes, J. Hone, H.L. Stormer, P. Kim, Phys. Rev. Lett. **101**, 096802 (2008)
23. C. Riedl, C. Coletti, U. Starke, J. Phys. D-Appl. Phys. **43**, 374009 (2010)
24. C. Berger, Z.M. Song, T.B. Li, X.B. Li, A.Y. Ogbazghi, R. Feng, Z.T. Dai, A.N. Marchenkov, E.H. Conrad, P.N. First, J. Phys. Chem. B **108**, 19912 (2004)
25. J. Hass, F. Varchon, J.E. Millan-otoya, M. Sprinkle, N. Sharma, C. Berger, P.N. First, L. Magaud, E.H. Conrad, Phys. Rev. Lett. **100**, 125504 (2008)
26. K.V. Emtsev, A. Bostwick, K. Horn, J. Jobst, G.L. Kellogg, L. Ley, J.L. McChesney, T. Ohta, S.A. Reshanov, J. Rohrl, E. Rotenberg, A.K. Schmid, D. Waldmann, H.B. Weber, T. Seyller, Nat. Mater. **8**, 203 (2009)
27. K.I. Bolotin, K.J. Sikes, Z. Jiang, M. Klima, G. Fudenberg, J. Hone, P. Kim, H.L. Stormer, Solid State Commun. **146**, 351 (2008)
28. S. Bae, H. Kim, Y. Lee, X.F. Xu, J.S. Park, Y. Zheng, J. Balakrishnan, T. Lei, H.R. Kim, Y.I. Song, Y.J. Kim, K.S. Kim, B. Ozyilmaz, J.H. Ahn, B.H. Hong, S. Iijima, Nat. Nanotechnol. **5**, 574 (2010)
29. Y. Hernandez, V. Nicolosi, M. Lotya, F.M. Blighe, Z.Y. Sun, S. De, I.T. McGovern, B. Holland, M. Byrne, Y.K. Gun'ko, J.J. Boland, P. Niraj, G. Duesberg, S. Krishnamurthy, R. Goodhue, J. Hutchison, V. Scardaci, A.C. Ferrari, Nat. Nanotechnol. **3**, 563 (2008)
30. M. Eizenberg, J.M. Blakely, Surf. Sci. **82**, 228 (1979)
31. P.W. Sutter, J.I. Flege, E.A. Sutter, Nat. Mater. **7**, 406 (2008)
32. A. Buchsteiner, A. Lerf, J. Pieper, J. Phys. Chem. B **110**, 22328 (2006)
33. R.Y.N. Gengler, K. Spyrou, P. Rudolf, J. Phys. D-Appl. Phys. **43**, 374015 (2010)
34. S. Stankovich, R.D. Piner, X.Q. Chen, N.Q. Wu, S.T. Nguyen, R.S. Ruoff, J. Mater. Chem. **16**, 155 (2006)
35. A.B. Kaiser, C. Gomez-navarro, R.S. Sundaram, M. Burghard, K. Kern, Nano Lett. **9**, 1787 (2009)
36. M. Lotya, Y. Hernandez, P.J. King, R.J. Smith, V. Nicolosi, L.S. Karlsson, F.M. Blighe, S. De, Z.M. Wang, I.T. McGovern, G.S. Duesberg, J.N. Coleman, J. Am. Chem. Soc. **131**, 3611 (2009)
37. Z.P. Sun, D. Popa, T. Hasan, F. Torrisi, F.Q. Wang, E.J.R. Kelleher, J.C. Travers, V. Nicolosi, A.C. Ferrari, Nano Res. **3**, 653 (2010)
38. H.A. Becerril, J. Mao, Z. Liu, R.M. Stoltenberg, Z. Bao, Y. Chen, ACS Nano **2**, 463 (2008)
39. R.R. Nair, P. Blake, A.N. Grigorenko, K.S. Novoselov, T.J. Booth, T. Stauber, N.M.R. Peres, A.K. Geim, Science **320**, 1308 (2008)
40. C. Lee, J.Y. Kim, S. Bae, K.S. Kim, B.H. Hong, E.J. Choi, Appl. Phys. Lett. **98**, 071905 (2011)
41. J.M. Dawlaty, S. Shivaraman, J. Strait, P. George, M. Chandrashekhar, F. Rana, M.G. Spencer, D. Veksler, Y.Q. Chen, Appl. Phys. Lett. **93**, 131905 (2008)
42. J. Horng, C.F. Chen, B.S. Geng, C. Girit, Y.B. Zhang, Z. Hao, H.A. Bechtel, M. Martin, A. Zettl, M.F. Crommie, Y.R. Shen, F. Wang, Phys. Rev. B **83**, 165113 (2011)
43. J.L. Tomaino, A.D. Jameson, J.W. Kevek, M.J. Paul, A.M. v d Zande, R.A. Barton, P.L. McEuen, E.D. Minot, Y. Lee, Opt. Express **19**, 141 (2011)
44. I. Maeng, S. Lim, S.J. Chae, Y.H. Lee, H. Choi, J. Son, Nano Lett. **12**(2), pp. 551–555 (2012). doi:10.1021/nl202442b

45. S.M. Kim, J.H. Jang, K.K. Kim, H.K. Park, J.J. Bae, W.J. Yu, I.H. Lee, G. Kim, D.D. Loc, U.J. Kim, E.H. Lee, H.J. Shin, J.Y. Choi, Y.H. Lee, J. Am. Chem. Soc. **131**, 327 (2009)
46. H. Choi, F. Borondics, D.A. Siegel, S.Y. Zhou, M.C. Martin, A. Lanzara, R.A. Kaindl, Appl. Phys. Lett. **94**, 172102 (2009)
47. H.N. Wang, J.H. Strait, P.A. George, S. Shivaraman, V.B. Shields, M. Chandrashekhar, J. Hwang, F. Rana, M.G. Spencer, C.S. Ruiz-vargas, J. Park, Appl. Phys. Lett. **96**, 081917 (2010)
48. J.M. Dawlaty, S. Shivaraman, M. Chandrashekhar, F. Rana, M.G. Spencer, Appl. Phys. Lett. **92**, 042116 (2008)
49. R.W. Newson, J. Dean, B. Schmidt, Opt. Express **17**, 2326 (2009)
50. P.J. Hale, S.M. Hornett, J. Moger, D.W. Horsell, E. Hendry, Phys. Rev. B **83**, 121404 (2011)
51. B.A. Ruzicka, S.A. Wang, L.K. Werake, B. Weintrub, K.P. Loh, H. Zhao, Phys. Rev. B **82**, 195414 (2010)
52. A. Borak, Science **308**, 638 (2005)
53. T. Kampfrath, L. Perfetti, F. Schapper, C. Frischkorn, M. Wolf, Phys. Rev. Lett. **95**, 187403 (2005)
54. A.C. Ferrari, J.C. Meyer, V. Scardaci, C. Casiraghi, M. Lazzeri, F. Mauri, S. Piscanec, D. Jiang, K.S. Novoselov, S. Roth, A.K. Geim, Phys. Rev. Lett. **97**, 187401 (2006)
55. J. Lloyd-Hughes, E. Castro-Camus, M.B. Johnston, Solid State Commun. **136**, 595 (2005)
56. A.G. Davies, E.H. Linfield, M.B. Johnston, Phys. Med. Biol. **47**, 3679 (2002)
57. F. Rana, Phys. Rev. B **76**, 155431 (2007)
58. T. Ohta, A. Bostwick, J.L. McChesney, K.V. Emtsev, A.K. Schmid, T. Seyller, K. Horn, E. Rotenberg, New J. Phys. **10**, 023034 (2008)
59. G.M. Rutter, J.N. Crain, N.P. Guisinger, T. Li, P.N. First, J.A. Stroscio, Science **317**, 219 (2007)
60. D.H. Auston, K.P. Cheung, J. Opt. Soc. Am. B-Opt. Phys. **2**, 606 (1985)
61. R.A. Kaindl, D. Hägele, M.A. Carnahan, D.S. Chemla, Phys. Rev. B **79**, 045320 (2009)
62. F. Rana, J.H. Strait, H.N. Wang, C. Manolatou, Phys. Rev. B **84**, 045437 (2011)
63. F. Rana, P.A. George, J.H. Strait, J. Dawlaty, S. Shivaraman, M. Chandrashekhar, M.G. Spencer, Phys. Rev. B **79**, 115447 (2009)
64. T. Winzer, A. Knorr, E. Malic, Nano Lett. **10**, 4839 (2010)
65. J.H. Strait, H.N. Wang, S. Shivaraman, V. Shields, M. Spencer, F. Rana, Nano Lett. **11**, 4902 (2011)
66. H. Suzuura, T. Ando, Phys. Rev. B **65**, 235412 (2002)
67. R. Bistritzer, A.H. MacDonald, Phys. Rev. Lett. **102**, 206410 (2009)
68. W.K. Tse, Phys. Rev. B **79**, 235406 (2009)
69. V. Ryzhii, M. Ryzhii, T. Otsuji, J. Appl. Phys. **101**, 083114 (2007)
70. S. Boubanga-tombet, S. Chan, T. Watanabe, A. Satou, V. Ryzhii, T. Otsuji, Phys. Rev. B **85**, 035443 (2012)
71. F. Rana, IEEE Trans. Nanotechnol. **7**, 91 (2008)
72. V. Ryzhii, A. Satou, T. Otsuji, J. Appl. Phys. **101**, 024509 (2007)
73. L. Ju, B.S. Geng, J. Horng, C. Girit, M. Martin, Z. Hao, H.A. Bechtel, X.G. Liang, A. Zettl, Y.R. Shen, F. Wang, Nat. Nanotechnol. **6**, 630 (2011)
74. A.R. Wright, X.G. Xu, J.C. Cao, C. Zhang, Appl. Phys. Lett. **95**, 072101 (2009)
75. W.S. Bao, S.Y. Liu, X.L. Lei, Phys. Lett. A **374**, 1266 (2010)
76. S.Y. Liu, N.J.M. Horing, X.L. Lei, IEEE Sens. J. **10**, 681 (2010)
77. L.W. Jiang, Y.S. Zheng, Phys. Lett. A **375**, 203 (2010)